Title

MICROANALYTICAL AND STRUCTURAL CHARACTERIZATION OF OPTICAL MATERIALS BY ELECTRON MICROSCOPY AND RELATED SPECTROCOPIES

Author

Krishnan, K.M.

Publication Date

1969-04-01

Lawrence Berkeley Laboratory
UNIVERSITY OF CALIFORNIA

Materials & Chemical Sciences Division

National Center for Electron Microscopy

Presented at the Materials Research Society Spring Meeting, "Optical Materials: Processing and Science," San Diego, CA, April 24–29, 1989, and to be published in the Proceedings

Microanalytical and Structural Characterization of Optical Materials by Electron Microscopy and Related Spectrocopies

K.M. Krishnan

April 1989

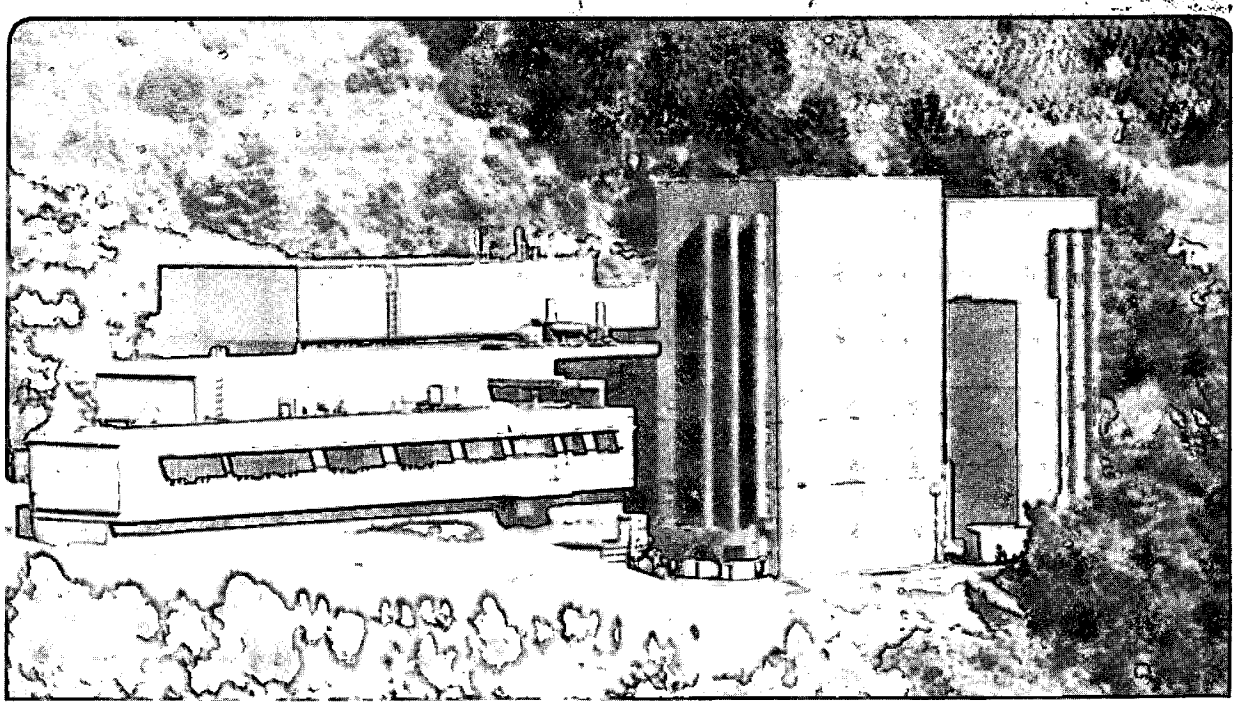

Prepared for the U.S. Department of Energy under Contract Number DE-AC03-76SF00098.

DISCLAIMER

MICROANALYTICAL AND STRUCTURAL CHARACTERIZATION OF OPTICAL MATERIALS BY ELECTRON MICROSCOPY AND RELATED SPECTROSCOPIES

KANNAN M. KRISHNAN
National Center for Electron Microscopy, Materials and Chemical Sciences Division, Lawrence Berkeley Laboratory, 1 Cyclotron Road, Berkeley, CA94720.

ABSTRACT

The fine probe forming capabilities of an analytical electron microscope combined with the development of related spectroscopies, diffraction and imaging techniques, makes it possible to obtain structural and chemical information from multiphase materials at high spatial resolution. These microanalytical methods are described with relevant examples from our studies of compounds in the Al_2O_3-AlN pseudobinary system, a potential window material, low-pressure synthesized diamond, diamond-like carbon and hydrocarbon films. A comprehensive example of the characterization of a novel AlON poltypoid structure (32H), illustrative of both the information content obtainable from these techniques at any particular level of resolution and the need to employ all the complementary methods of analysis, is discussed. Efforts to characterize a variety of diamond-like carbon films by the measurements of both the low-loss plasmon resonances and the fine structure in the core-loss edges observable in the energy-loss spectrum, to obtain sp^3/sp^2 ratios are outlined. The electronic structure of thin film diamonds, synthesized by a plasma enhanced chemical vapour deposition method, has been shown to be in agreement with band structure calculations.

INTRODUCTION

The development and potential utilization of materials for optical applications is dependent on a systematic effort involving processing, characterization and appropriate property measurements. The methods of characterization are numerous and it is important to employ the one that is appropriate to the problem both in terms of its information content and the achievable level of resolution. With the incorporation of fine probe forming capabilities in a transmission electron microscope and the development of related diffraction, imaging and spectroscopic methods, it is now possible to obtain structural and chemical information from the same region of the sample at high spatial resolution. Recent advances in these microanalytical methods discussed in this paper include, high resolution electron microscopy (HREM), convergent beam electron diffraction (CBED), energy dispersive x-ray spectroscopy (EDXS) with particular emphasis on low atomic number element microanalysis, and electron energy-loss spectroscopy (EELS). Applications of these methods to the study of the crystallography and phase stability of defective structures in the Al_2O_3-AlN pseudobinary system (an optical window material with excellent mechanical properties), detemination of sp^3/sp^2 ratios in diamond-like carbon and hydrocarbon films and the study of thin film diamonds synthesized by a low pressure chemical vapour deposition process are discussed.

OVERVIEW OF ELECTRON-OPTICAL CHARACTERIZATION METHODS

The interaction of a fast electron, accelerated through kilovolt potentials in an electron microscope, with a thin foil will produce a variety of signals that can be monitored with appropriate detectors to provide a wealth of information about the crystallography, chemistry and electronic structure of the sample. The structural and crystallographic information is contained in the elastically scattered beams and can be effectively interpreted either by the measurement of the electron diffraction patterns or by recording the diffraction contrast (conventional) and phase contrast (high resolution) images. If the incident beam is focussed exactly at the specimen surface and a cone-like convergent probe is used (CBED), each of the nominal diffraction spots now appear as discs due to the wider angular view (figure 1). In addition, because of the wide range of incident beam orientations (similar to a rocking curve measurement in x-ray diffraction), higher order Laue zone (HOLZ)

reflections, representative of the periodicity in the direction perpendicular to the specimen surface, are also observed (figure 3). In addition, the elastic interaction between the discs in the ZOLZ and the HOLZ give rise to a set of fine features within each of the discs in the ZOLZ. The symmetry of the features in the central transmitted disc (BF), the whole pattern symmetry (WP), and the symmetry within each dark field order when set at its Bragg condition (DF), can be compared to a set of tables belonging to all possible crystal point groups to unequivocally identify the crystal structure [1]. Another consequence of working with such a convergent probe is the improvement in spatial resolution as the smallest possible area in the sample can be studied. In addition, the microstructure can be imaged either by selecting one of the diffracted beams (diffraction contrast) or by combining many diffracted beams using a large aperture to obtain a high resolution phase contrast image. A typical high resolution image, obtained using the atomic resolution microscope at the NCEM, is shown in figure 7.

In addition to the above, the inelastically scattered fast electron distribution and the multitude of emissions produced by the response of the sample to its excitation by the incident electron beam, incorporate the chemical and electronic structure information. In particular, the de-excitation processes such as characteristic x-ray emissions, are well understood and their measurements form the basis of the widely used EDXS technique of microanalysis. A typical EDX spectrum, acquired with a Si(Li) detctor fitted with an ultra-thin window, is shown in figure 4. The measured characteristic x-ray intensities (I_A,I_B) can be related to the elemental weight fractions (C_A,C_B) using the ratio method proposed by Cliff and Lorimer [2],

$$C_A/C_B = (K_B\, I_A) / (K_A\, I_B) = K_{AB}\, (I_A/I_B) = (K_{ASi}/K_{BSi})\,)(I_A/I_B) \qquad (1).$$

These K-kactors, K_{AB} are normally determined with respect to silicon. The term K_A for any particular element A is a product of the relevant x-ray generation parameters and an instrument-dependent efficiency parameter. It is possible to calculate these K-factors if the cross section used for inner shell ionizations are reliable and the detector and window parameters that determine the efficiency are well known. These K-factors can also be determined experimentally for a particular microscope operating at a fixed acceleration voltage, provided suitable thin film standards can be obtained. This experimental approach is essential for the quantification of low atomic number elements, such as boron, carbon, nitrogen and oxygen, because of the significant absorption of the low energy characteristic x-rays in both the sample and the detector. These K-factors have been systematically measured (figure 5) and used routinely in our laboratory [3]. An example of the determination of the cation/anion ratio using these experimentally measured K-factors is discussed in a subsequent section .

The transmission electron energy-loss spectrum can provide a wealth of information about the bonding and electronic structure of the sample [4]. A representative EEL spectrum for diamond is shown in figure 6. The low-loss region consists of broad resonance peaks called plasmons and represent the collective excitation of the delocalized outer shell electrons by the primary beam. In a simple jellium or free electron gas model the plasmon energy is proportional to the square root of the number density of electrons in the thin film [5]. In the case of carbon, the plasmon peak positions appear at different energies depending on its form. These peak positions are reproducible and might provide some clues to the structural characterization of diamond-like carbon films. In addition, by performing a Kramer-Kronig analysis of the low loss region the optical constants ε_1 and ε_2 can be evaluated. A ratio of the fraction of π to σ electron in the carbon films can also be obtained by a sum rule calculation. Alternatively, the higher energy core-loss features also incorporate the electronic and bonding information. The onset of the edge is a function of both the initial state and the position and nature of the vacant state at the Fermi level. Band gaps can easily be resolved. The near edge fine structure can be interpreted in terms of either a multiple scattering method or a single particle pseudo-atomic-orbital band theory method [22].

Finally, each of these techniques have well defined limits of spatial resolution. It is possible that structural and chemical measurements may be averaged over the areas of investigation leading to significant variations in interpretations. An example of this is given in a later section.

Sintered aluminium oxynitride has the potential of being a durable low-cost window material and is transparent to ultraviolet, visible and infrared wavelengths [6]. From 0.3 to 5.0 μm, the minimum in-line transmission is 74%. Sintering in N_2 occurs at 1900-2000°C and 98% of the theoretical density can be achieved. The material also exhibits good mechanical properties: elastic modulus of 3.2×10^5 MPa, Knoop hardness of 1800 Kg/mm^2, flexural strength of 256MPa and a thermal expansion coefficient of 7.0×10^{-6}/°C have been measured.

Pure single crystal aluminium oxide is an anisotropic material and exhibits directional variation in optical and thermal properties. True optical transparency of polcrystalline Al_2O_3 is impossible unless all the grains are identically oriented. Further significant strains can arise due to the thermal expansion mismatch at the grain boundaries. An alternative simpler approach is the stabilization of cubic Al_2O_3 by the addition of nitrogen, in the form of AlN, to form defective spinels. To sinter such fully dense single phase ceramics it is essential to refine the temperature-composition stability limits of nitrogen stabilized cubic aluminium oxide (ALON) and to fully characterize the final reaction products by TEM.

Sintering and phase equilibria of the Al_2O_3 -AlN pseudo-binary system were studied in detail [7]. There is a relatively wide range of compositional stability, roughly centered at 35.7 mol% AlN and a maximum in thermal stability at 2050 °C. At this point ALON seems to melt incongruently into one alumina-rich, stable liquid and one nitride-rich, unstable liquid. Using a constant anion spinel model the ALON composition was predicted to be 35.7 mol% AlN.

A set of CBED patterns of this ALON phase are shown in figure 1. The whole pattern and the central transmitted disc exhibit 4mm symmetry. The (400) dark field order when set at the Bragg condition exhibits 2mm symmetry. The (220) and (220) reflections are related by a two fold rotation. By comparing these observations with the tables of Buxton et al it can be concluded that this material has a projected diffraction group of $4mm1_R$ and a point group of m3m. The displacements of the position of the FOLZ discs with respect to the ZOLZ disc confirms that the material is indeed face centered cubic. This crystallographic confirmation of a cubic spinel structure is corroborated by the measured optical transmission over a broad range of wavelengths.

Unfortunately, most AlN powders contain some oxygen impurities and therefore such sintering processes result in materials with polytype-like phases of AlN [8]. These polytypoids result from the insertion of a chemically distinct layer into another chemically distinct structure, i.e. a cubic layer of local composition MX_2 (where M is the cation and X is the anion), inserted in the hexagonal AlN (or MX) stacking sequence. The periodicity of such faulting, that defines the character of this modulated structure, is a function of the overall composition and constrained by charge balance. The system Al_2O_3-AlN is a pseudobinary composition join in the three element Al-N-O system, and the phase rule allows for phase fields with three coexisting phases. There is an intimate relationship between liquid formation and the appearance of the various polytypoids. Further, the morphologies of the polytypoids are variable and seem to reflect the difficulty in attaining equilibrium. Hence, it is important to characterize these polytypoids to obtain an understanding of the phase equilibria in this part of the phase diagram and relate it to the processing and properties of these materials [6].

Figure 2 shows a selected area diffraction pattern, conventional lattice image and an optical diffractogram from a region of the 32H polytypoid structure. The position of the (010) spot with respect to the transmitted beam in the SAD confirms the hexagonal stacking sequence. From this SAD pattern, the repeat distance along the c-axis can be calculated to be 8.3nm for this structure. However, both the lattice image and the accompanying optical diffractogram show a spacing of 4.3nm. This is not a surprising discrepancy, for the nH polytypoids in this system normally consist of two blocks of n/2 layers related by a c-glide plane. This is verified in Figure 3, which shows a CBED pattern oriented such that the c-axis is parallel to the incident beam. The diameter G_1 of the first order Laue zone (FOLZ) in such

a pattern can be related to this repeat distance [9], and is given by the expression

$$G_1 = (2KH)^{1/2} \quad (2)$$

where K= $1/\lambda$ and H for a hexagonal structure is

$$H = [a^2 (U^2+V^2 -UV) + c^2W^2]^{-1/2} . \quad (3)$$

Here U,V, W are the direction indices in the four-index Miller-Bravais system and a,c are the hexagonal lattice parameters. From the radius of the FOLZ ring, using equations (2) and (3), the periodicity along the c-axis is calculated to be 4.2nm. However, this CBED pattern was obtained with a 60nm diameter probe and the information is averaged over many unit cells. However, if these polytypoids are compositionally stabilized, it is predicted that the anion/cation ratio should be 17/16 or 1.06. A typical EDX spectrum obtained from a 32H region of the sample is shown in Figure 4. The experimentally measured characteristic x-ray intensities can be related to the actual composition by the Cliff-Lorimer relationship. Such an analysis, carried out using experimentally measured K-factors, suggests a composition of 47.9 at.% Al, 13.8 at.% O and 38.3 at.% N. The experimental error in these measurements is approximately $\pm$2 %. Note that the anion/cation ratio obtained from this measurement, i.e. 1.08, agrees well with the predicted value, confirming the stability of such a long period polytypoid. However, if direct imaging of the structure with atomic resolution is used (Figure 7), the periodicity along the c-direction can be shown to be a sequence of alternate 7:9:7:9 ... repeats . This result can be interpreted as parallel intergrowths of the 27R (c = 7.2 nm) and 21R (c = 5.7 nm) polytypoids. Clearly adjacent units of 21R and 27R add up to the 32H repeat units. A detailed interpretation of these images would require simulations of the image based on a predicted structural model for the intergrowths. Such image calculations using the multislice method [10] are currently in progress.

DIAMOND-LIKE CARBON FILMS

There is substantial interest in diamond films because of their extreme properties [11]. In particular, it is a wide band gap semiconductor with desirable optical properties, i.e. no absorption in the visible region. However, its properties are strongly dependent on impurities and other lattice defects. The growth of diamond films at low pressures, where it is metastable, has received considerable attention in recent times [12,13]. A variety of methods including ion beam deposition, chemical vapour deposition and plasma deposition have been employed. In general, " diamond-like" carbon (variously referred to as DLC, a-C, i-C, etc.) or hydrocarbon (DLHC, a-C:H, etc.) with properties approaching that of diamond are commonly produced. The properties of such DLC and DLHC films vary widely and this variation is believed to be a function of the nature of the carbon-carbon bonds or the electronic structure of the carbon atoms [14]. Cubic diamond has sp^3 carbon with tetrahedral coordination. On the other hand, graphite has sp^2 and a layered structure with strong σ bonding in the sheets and weak π bonding in between. Both DLC and DLHC films include a varying range of sp^3/ sp^2 hybridized carbon atom ratio, but with no long range crystalline order. The microstructure of such DLC and DLHC films have been characterized by a variety of methods. These include Raman spectroscopy [15], X-ray diffraction, TEM and various surface analytical techniques [16]. However, there is no established correlation between these various methods. Such correlations are important for the characterization of thin films with small polycrystalline grains where established methods such as Raman spectroscopy are misleading, and high spatial resolution methods such as electron energy-loss spectroscopy in a transmission electron microscope are in need of further investigation.

The low energy-loss spectra from a variety of different forms of carbon are shown in figure 8. In addition to standards, such as highly oriented pyrolitic graphite and natural diamond, spectra from evaporated carbon, DLC and DLHC films are shown. The DLC and DLHC films were prepared by reactive dc magnetron sputtering. The DLHC film was prepared with approximately 20% hydrogen mixed in with argon. These two films exhibit remarkably different optical properties. The DLC film has a visible and solar transmittance of

0.2 and 0.35, respectively. The DLHC film has $T_V = 0.86$ and $T_S = 0.87$ [17]. For layered sp^2 structures, two prominent plasmon resonances are observed. They involve either the π band lying close to the Fermi level or a combination of the $\sigma+\pi$ bands. For natural sp^3 diamond a single peak at 35.2 eV and a shoulder at 24.8 eV are measured. The feature at 24.8eV is reproducible but is due to amorphous carbon layers on the surface, possibly due to electron or ion beam damage, and is thickness dependent. The evaporated carbon has a broad peak at 25.5eV. Both DLC and DLHC films show the π and $\sigma+\pi$ resonances. However, the resonances are shifted to lower energies for the DLHC film. The difference in the energy shifts (0.9 eV for $\sigma+\pi$ and 2eV for π) reflects a quantitative change in the number density of π and σ electrons , as the plasmon resonance energy is directly proportional to $n^{1/2}$, where n is the appropriate electron density in a nearly-free electron gas model. However, the magnitude of these shifts is too small to be of any significance. Alternatively, as the energy-loss spectrum is proportional to $\mathrm{Im}(-1/\epsilon)$, the ratio of π to σ bonded electrons can be determined by a sum rule calculation [18]. Such work is currently in progress, but there is considerable ambiguity in determining the range of the integrals for the σ and π contributions.

The structural information can also be derived from measurements of the characteristic core-loss edges. The fine structure near the onset of the edges, reflecting the density of unoccupied states, is sensitive to sp^2 and sp^3 carbon. The core edges for all the forms of carbon discussed earlier are shown in Figure 9. Graphite exhibits strong π^* and σ^* features at 285.5eV and 292eV respectively. The onset of the σ^* in diamond is shifted by 5.5eV from the π^* in graphite and is determined by the band gap. The DLC and DLHC films exhibit sharp π^* features, followed by a broad σ^* edge. The ratio of the heights (π^*/σ^*) is smaller for the DLHC film indicating a larger diamond contribution. This is in agreement with the enhanced optical transmission discussed earlier. These interpretations are only qualitative. Quantitative results can be obtained only if such measurements are standardized with studies of materials with known sp^3/sp^2 ratios or by a systematic comparison of the results from complemetary techniques.

DIAMOND THIN FILMS

Samples were obtained from Pennsylvania State University. Thin films of diamond approximately 1μm thick were deposited on fused silicon dioxide substrates by a plasma enhanced chemical vapour depoition method [19]. Preliminary characterization of the films by scanning electron microscopy showed a micron sized polycrystalline film with a large number of threefold {111} facets. Raman spectroscopy, exhibited the characteristic diamond line at 1332 cm^{-1}. A typical TEM micrograph of a plan view sample, prepared by ion milling from only the side of the substrate, is shown in figure 10. The material has a high density of defects, particularly {111} type microtwins. These twins have been studied extensively by HREM, using the atomic resolution microscope at the NCEM. The results of that study will be published in a separate article [20]. The diamond crystal structure of these grains was confirmed by both conventional electon diffraction (figure 10, inset) and by using a convergent probe of 10nm diameter. The lattice parameters obtained from this measurement, i.e. 0.205 nm, 0.178 nm, 0.125nm and 0.107 nm for (111), (200), (220) and (311) respectively, are in good agreement with the values in the literature. The four unindexed spots correspond to the (111) planes in the adjacent grain. Hence, all the spots are accounted for in the diffraction patterns. This is in contrast with an earlier work where the presence of an intermediate phase of SiC was invoked to account for additional reflections in the diffraction pattern [21]. Moreover, in our samples no intermediate phase was observed in either high resolution imaging or diffraction work using cross-section samples.

The bonding of carbon in such films is critical to their properties. Therefore it is essential to unequivocally identify that these films are made of sp^3 carbon and the π bonding is negligible or totally absent. Electron energy-loss spectra from the thin film diamond sample, along with those of graphite and natural diamond standards, are shown in figure 11. It can be seen that the spectra of the low pressure diamond and the natural diamond standard, both in terms of the onset of the edge which is determined by the band gap and the near edge fine structure, are in good agreement with each other. In the same figure results of some

recent calculations of the fine structure of electron energy loss edges are also shown. The results of a multiple scattering (MS) method and a single particle self-consistent pseudo-atomic-orbital band theory (p-DOS) method are included. The p-DOS calculation is in good agreement with the experimental spectrum of low pressure diamond; peaks at 292eV, 298.7 eV, 305.7eV and 308.1eV are predicted in the theory and observed in the experiment. This confirms that the material is indeed diamond. However, a faint π^* feature may be present at 286eV at the onset of the edge. This is better shown in figure 12 - the π^* feature can be clearly seen above the calculated background. This could be due to the presence of amorphous carbon either at the grain boundaries between diamond grains or at the surface of the diamond film. A typical grain boundary is shown in figure 10. We failed to identify any such amorphous films at the grain boundaries in our prelimnary HREM measurements. It must also be pointed out that the preparation of electron transparent thin foils of diamond is difficult and the method of ion beam milling could result in surface damage of the film. However, substantial difference in the resistivity of such films, depending on the position of the substrate with respect to the plasma, is observed [23]. This has been attributed to the possible incorporation of π-bonded carbon at the grain boundaries. The identification of such layers, if they are indeed present, would explain the electrical properties of these films. Such work is currently in progress.

ACKNOWLEDGEMENTS

The author would like to thank Dr. J. W. McCauley of AMMRC for supplying the ALON materials, Dr. M. Rubin of LBL for supplying the DLC films and for sharing the results of their optical property measurements, Mr. D. Pickrell of Pennsylvania State University for supplying the thin film diamonds, Mr. C. J. Echer for assistance on the 200CX AEM and Mr. J. H. Turner for photography. The work was supported by the Director, Office of Energy Research, Office of Basic Energy Sciences, Materials Science Division of the U.S. Department of Energy under contract #DE-AC03-76SF00098.

REFERENCES

1. B. F. Buxton, J. A. Eades, J. W. Steeds, G. M. Rackham, Phil. Trans. Roy. Soc. A281, 171 (1976).
2. G. Cliff and G. W. Lorimer, J. Micros. 103, 203 (1975).
3. K. M. Krishnan and C. J. Echer, in Analytical Electron Microscopy, D.C. Joy editor, San Francisco Press, 99 (1987).
4. R. F. Egerton, EELS in the EM, Plenum Press, New York (1986).
5. H. Raether, Excitations of Plasmons and Interband Transitions by Electrons, Springer Verlag Press, New York (1980).
6. T. M. Harnett et al., Cearmic Engineering and Science, 3, 67 (1982).
7. J. W. McCauley and N. D. Corbin, J. Am. Cer. Soc. 62, 476 (1979).
8. K. H. Jack, J. Mat. Sci. 11, 1135 (1976).
9. J. Steeds in Introduction to AEM, edited by Hren, Goldstein and Joy, Plenum Press, New York (1979).
10. M.A. O'Keefe and R. Kilaas, in Image and Signal Processing in Electron Microscopy, P. W. Hawkes, F. P. Ottensmeyer, A. Rosenfeld, W. O. Saxton editors, 225 (1988).
11. J. C. Angus and C. H. Hayman, Science 241, 913 (1988).
12. R. C. DeVries, Ann. Rev. Mater. Sci. 17, 161 (1987)
13. V. P. Varnin, I. G. Teremenskaya, D.V. Fedoseev and B. V. Deryaguin, Sov. Phys. Dokl. 29, 419 (1984).
14. H. Tsai and D. B. Bogey, J. Vac. Sci. Tech. A5, 3287 (1987).
15. D. S. Knight and W. B. White, J. Mater. Res. 4,385 (1989).
16. S. R. Kasi, H. Kang, J. W. Rablais, J. Chem. Phys. 88, 5914 (1988).
17. M. Rubin, private communication.

18. J. Fink et al , Phys. Rev. B30, 4713 (1984).
19. A. R. Badzian, T. Badzian, R. Roy, R. Messier, K.E. Spear, Mat. Res. Bull. 23, 531 (1988).
20. K. M. Krishnan and C.J. D. Hetherington, unpublished data.
21. B. E. Williams and J. T. Glass, J. Mat. Res. 4, 373 (1989).
22. X. Weng, P. Rez and H. Ma, Phys. Rev B, in press
23. D. Pickrell, private communication.

Fig. 1: A set of convergent beam electron diffraction patterns at the <100> orientation for a 35.7 mol% AlN-Al_2O_3 sample. Based on the work of Buxton et al. [1], the symmetries of these patterns confirm that the sample is indeed cubic with the m3m point group. The isotropic optical properties of this cubic phase allows the use of a polycrystalline material for window applications.

Fig 2: Selected area diffraction pattern, lattice image and optical diffractogram from the hexagonal long period polytypoid structure. The diffraction pattern suggests a unit cell parameter c=8.4nm. The lattice image shows a structural regularity of 4.3nm.

Fig 3: A CBED pattern in the <0001> orientation for the above polytypoid. The diameter of the FOLZ gives the periodicity of faulting in the c-direction as 4.2nm in agreement with the lattice image. Based on these measurements, the structure has been identified as a 32H polytypoid, with c=8.4nm, but with a glide plane at half the unit cell parameter.

Fig. 4: A typical EDXS spectrum. The composition is determined from integrated intensities using experimental proportionality or K-factors. Absorption corrections are included. This measurement confirms that the 32H polytypoid is compositionally stabilized.

Fig. 5: Experimentally measured K-factors for the ultra-thin window Si(Li) detector. The window parameters used in the theoretical modelling are also shown. A 200kV acceleration voltage was used for all measurements.

Fig. 6: Energy-loss spectrum of natural diamond. Features of interest include low-loss plasmon resonances and higher energy characteristic core-loss edges.

Fig. 7: A HREM image of the 32H poytypoid structure obtained on the atomic resolution microscope. The 16 layer repeat structure is shown to be an intergrowth of 9 and 7 layer repeats.

Fig. 8: Comparison of the low-loss plasmon resonances of a) evaporated carbon, b) diamond-like carbon, c) diamond-like hydrocarbon, d) highly oriented pyrolitic graphite and e) natural diamond. The sp^2 carbon shows two resonances: π and $\sigma+\pi$.

Fig. 9: The core-loss profile of the C-K edge for the different forms of carbon discussed in figure 8. The ratio of the heights of the π^* to σ^* features, could potentially be used to obtain sp^3/sp^2 ratios, but so far it has been difficult to obtain consistent measurements. Standards of known ratios, made with C^{13} to facilitate comparison with NMR measurements are currently being synthesized to overcome these difficulties.

Fig. 10: A typical microstructure of thin film diamond synthesized by plasma CVD methods. A high density of microtwins on the (111) planes are observed. The diffraction pattern (insets) confirms the diamond crystal structure. The twin spots are indexed separately and the streaking is due to the close proximity of neighbouring microtwins.

Fig. 11: The C-K edge profiles of plasma CVD diamond, HOPG and natural diamond. The fine structure of the diamond is in good agreement with recent theoretical predictions based on a projected density of states (p-DOS) method [22]. However, a faint π^* peak, representative of sp^2 carbon is present.

Fig. 12: The π^* peak observed above is well resolved above the background. It is believed that this feature is due to the electron beam damage of the diamond film.

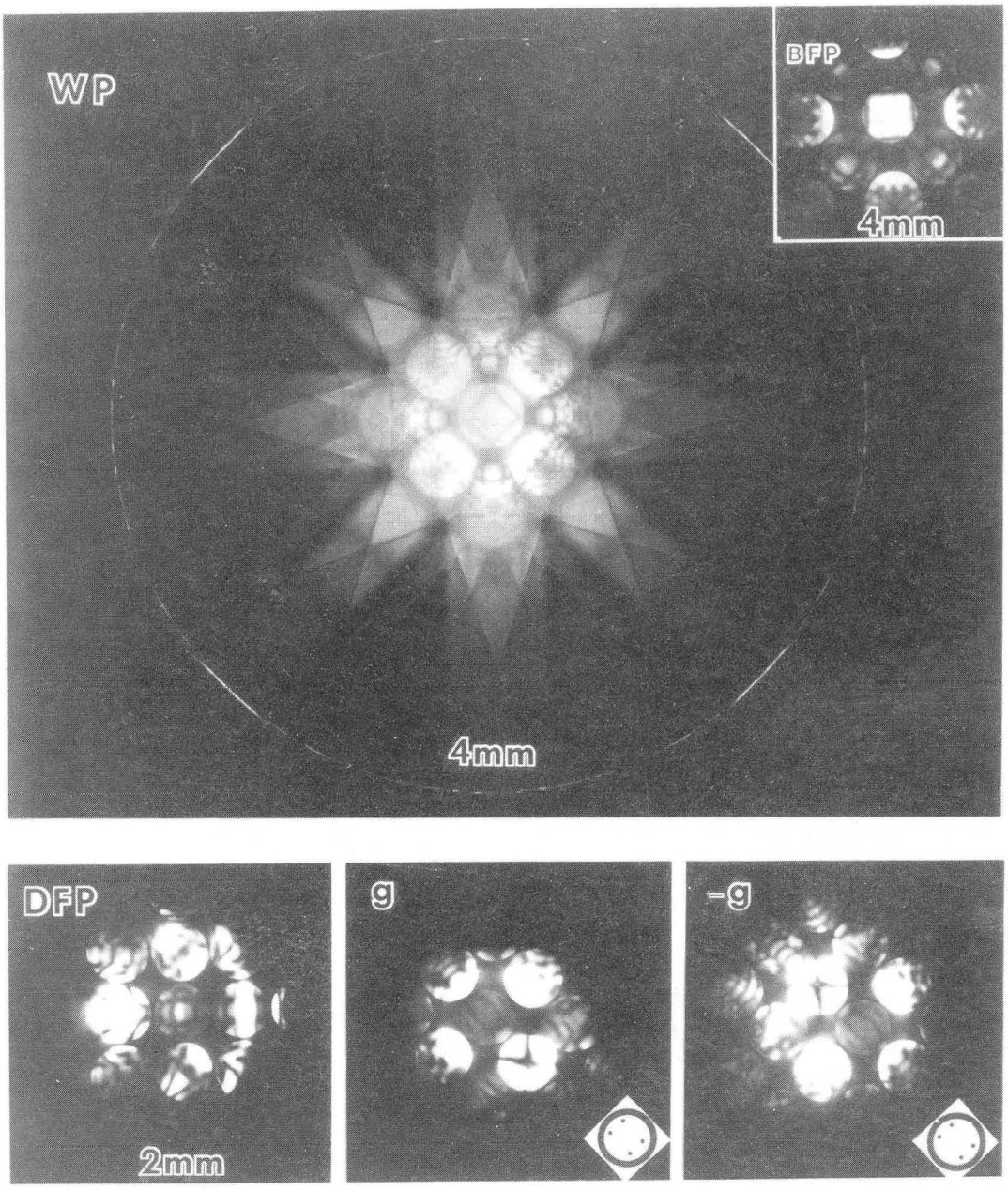

XBB 856-4534

Figure 1

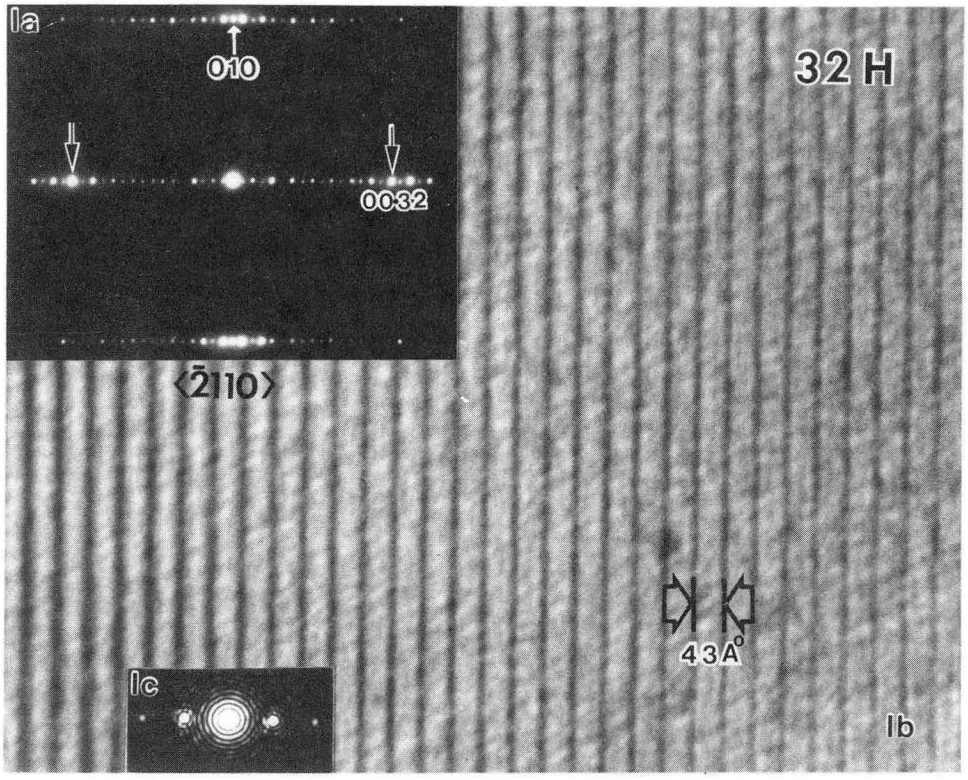

XBB 872-960

Figure 2

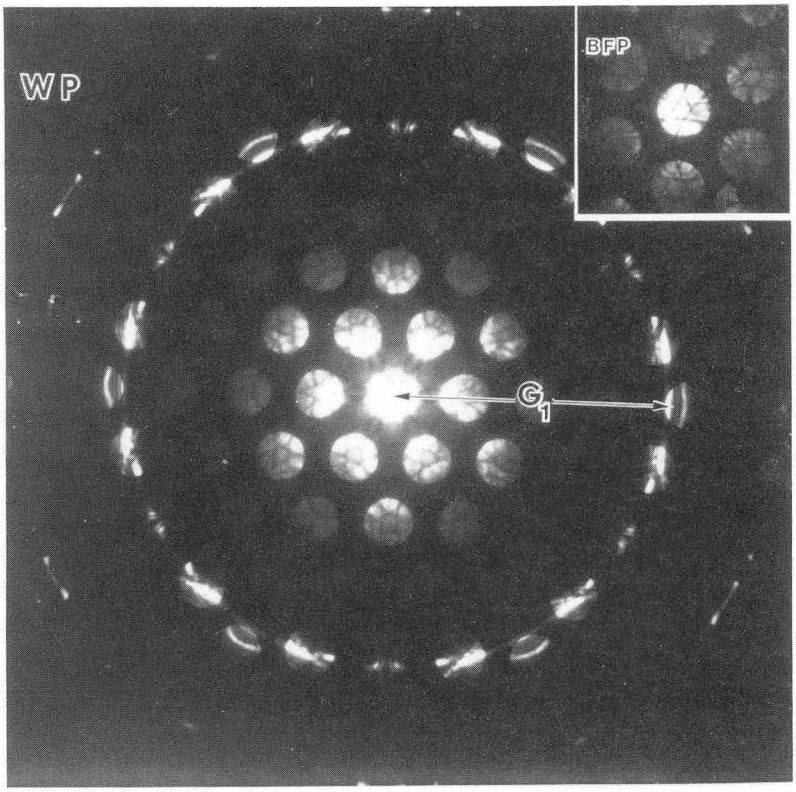

XBB 856-4533

Figure 3

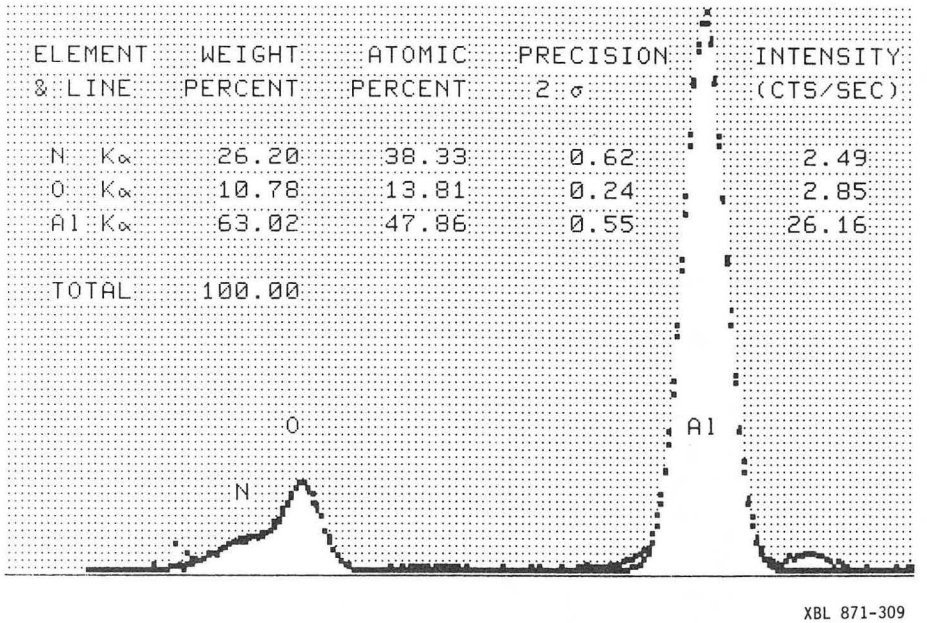

XBL 871-309

Figure 4

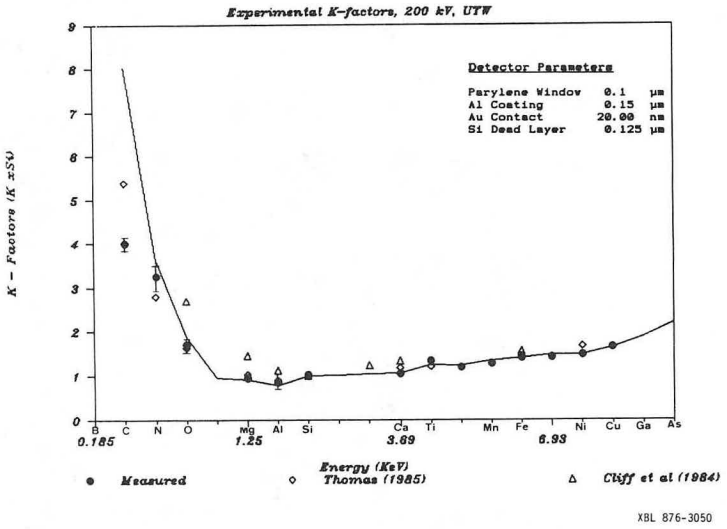
Experimental K-factors, 200 kV, UTW
K - Factors (K xSi)
Detector Parameters
Parylene Window 0.1 µm
Al Coating 0.15 µm
Au Contact 20.00 nm
Si Dead Layer 0.125 µm
B C N O Mg Al Si Ca Ti Mn Fe I Ni Cu Ga As
0.185
1.25
3.69
6.93
Energy (KeV)
Measured
Thomas (1985)
Cliff et al (1984)
XBL 876-3050

Figure 5

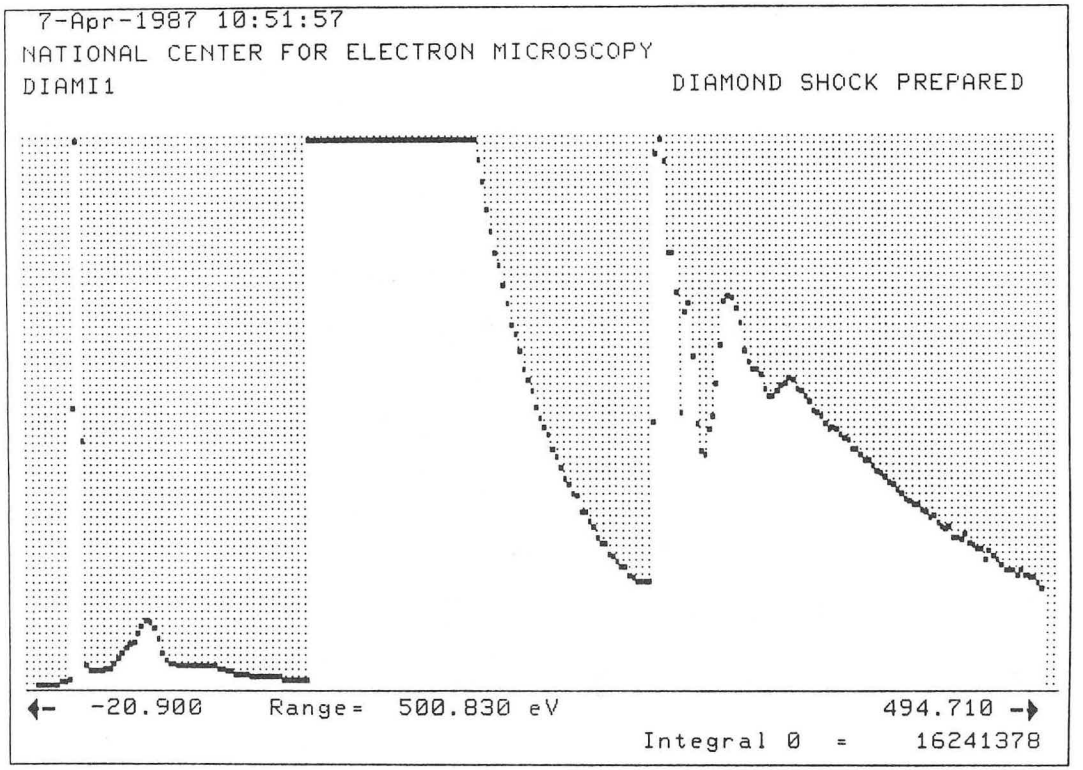
7-Apr-1987 10:51:57
NATIONAL CENTER FOR ELECTRON MICROSCOPY
DIAMI1
DIAMOND SHOCK PREPARED
-20.900
Range= 500.830 eV
494.710
Integral 0 = 16241378
XBL 878-3699

Figure 6

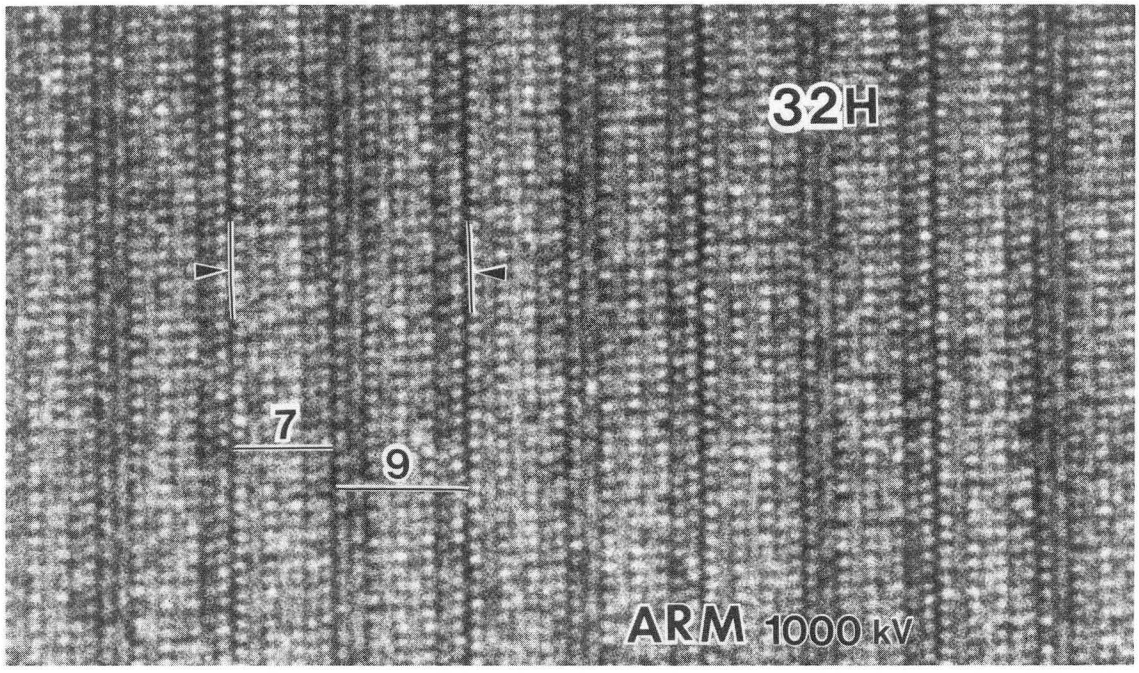

XBB 872-959

Figure 7

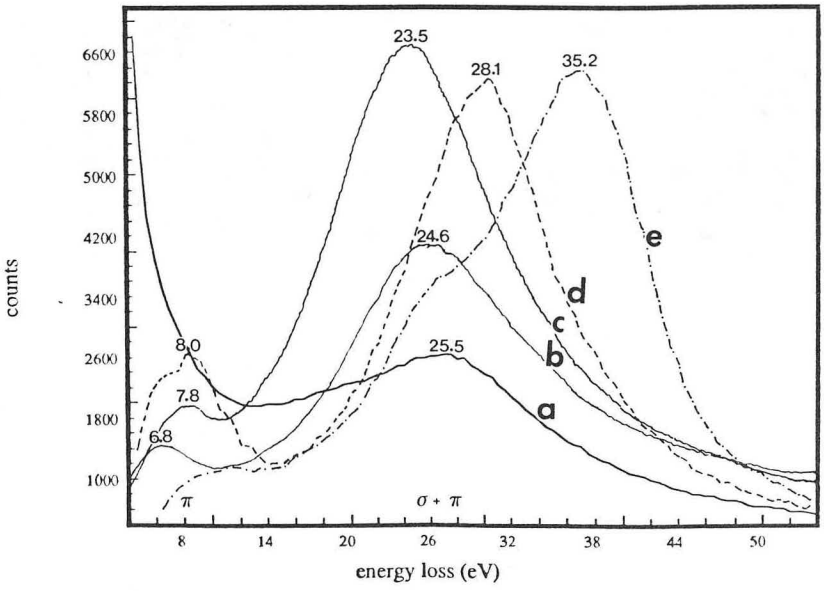
counts
6600
5800
5000
4200
3400
2600
1800
1000
23.5
28.1
35.2
24.6
8.0
7.8
6.8
25.5
a
b
c
d
e
π
σ + π
8
14
20
26
32
38
44
50
energy loss (eV)
XBL 894-1466A

Figure 8

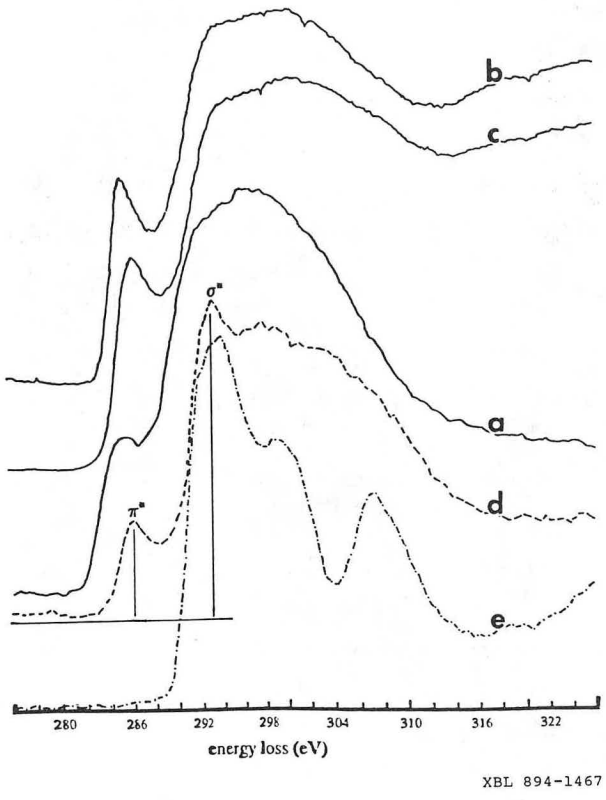
b
c
a
d
e
σ*
π*
280
286
292
298
304
310
316
322
energy loss (eV)
XBL 894-1467

Figure 9

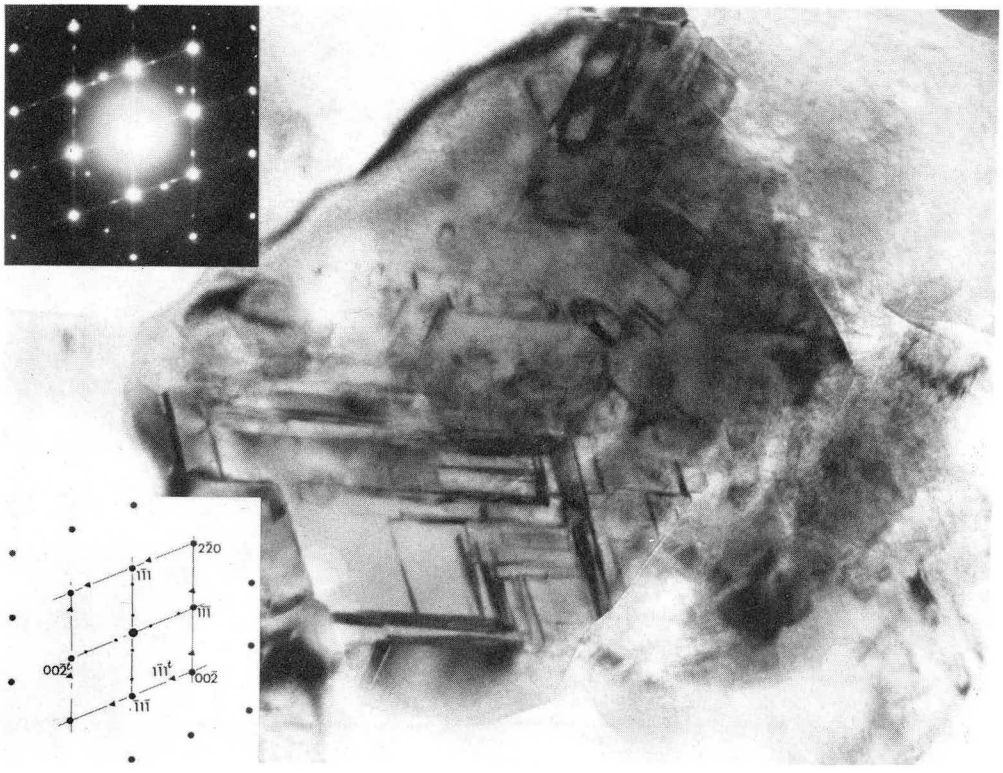

XBB 894-3261

Figure 10

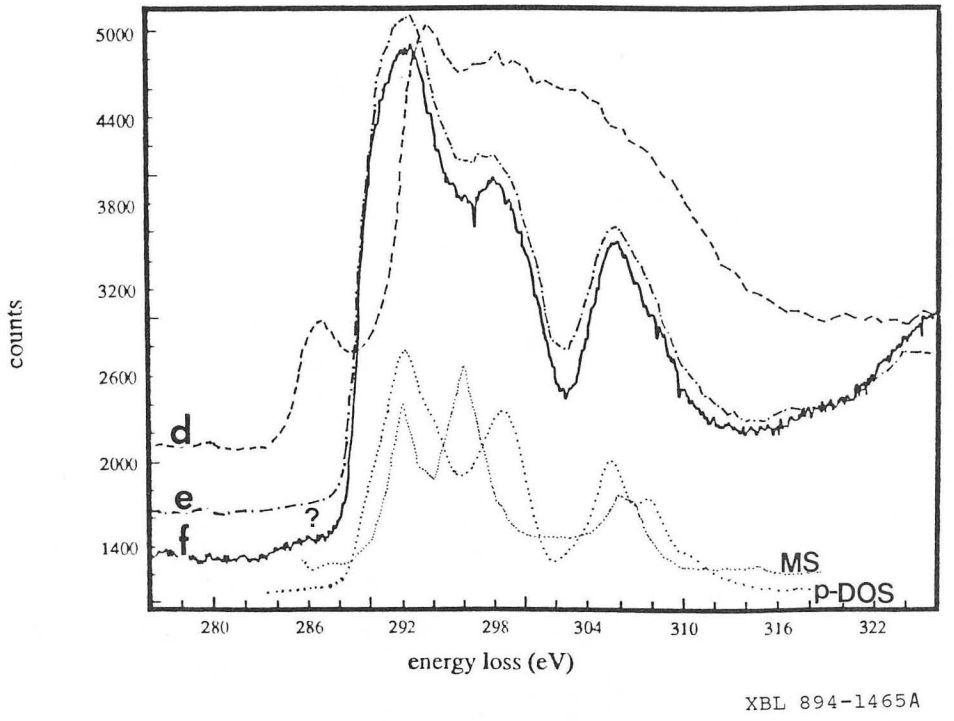
counts
5000
4400
3800
3200
2600
2000
1400
d
e
f
?
MS
p-DOS
280
286
292
298
304
310
316
322
energy loss (eV)
XBL 894-1465A

Figure 11

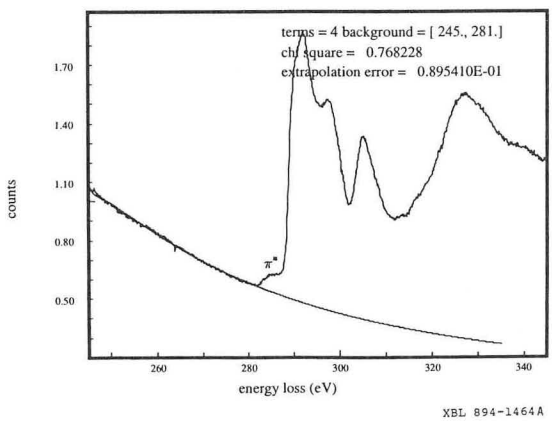
terms = 4 background = [245., 281.]
chi square = 0.768228
extrapolation error = 0.895410E-01
1.70
1.40
1.10
0.80
0.50
counts
π*
260
280
300
320
340
energy loss (eV)
XBL 894-1464A

Figure 12

LAWRENCE BERKELEY LABORATORY
TECHNICAL INFORMATION DEPARTMENT
1 CYCLOTRON ROAD
BERKELEY, CALIFORNIA 94720